# MEMS IMU for AHRS Applications

W. Geiger, J. Bartholomeyczik, U. Breng, W. Gutmann, M. Hafen, E. Handrich, M. Huber, A. Jäckle, U. Kempfer, H. Kopmann, J. Kunz, P. Leinfelder, R. Ohmberger, U. Probst, M. Ruf, G. Spahlinger, A. Rasch, J. Straub-Kalthoff, M. Stroda, K. Stumpf, C. Weber, M. Zimmermann, S. Zimmermann

Northrop Grumman, Electronic Systems, LITEF GmbH, 79115 Freiburg, Germany

***Abstract*—Northrop Grumman, LITEF is developing MEMS (Micro-Electro-Mechanical Systems) based Inertial Measurement Units (IMU) for future Attitude and Heading Reference Systems (AHRS) with a target accuracy of 5 °/h for the gyroscopes and 2.5 mg for the accelerometers. Within the technology development phase, prototype single axis gyroscopes have been realized and extensively tested for effects including temperature, acoustic and vibration sensitivities. These devices employ micro-machined all-silicon gyroscope sensor chips processed with Deep Reactive Ion Etching (DRIE). Silicon fusion bonding ensures pressures smaller than $3 \cdot 10^{-2}$ mbar. Sophisticated analog electronics and digital signal processing condition the capacitive pick-off signals and realize full closed loop operation. The current results with overall bias error smaller than 2 °/h to 5 °/h, scale factor error <1200 ppm, measurement range >1000 °/s and angular random walk <0.4 °/√h indicate that stable production of 5 °/h gyroscopes is realistic. The fabrication technology for capacitive, pendulous accelerometer chips is based on that used for the gyros with only an increase in the enclosed pressure to obtain overcritical damping. Pulse Width Modulation (PWM) within a digital control loop is used to realize closed loop operation. Accelerometer chips have been tested over temperature with a residual bias error <2.0 mg and a scale factor error <1400 ppm. These sensor chips have been integrated into an IMU whereby the power budget and size of the sensor electronics have been optimized. In this paper the salient features of the gyro and accelerometer designs are presented together with an overview of the IMU system architecture. Measurement results, with a focus on environmental characteristics and robustness, are included.**

## I. Introduction

Attitude and heading reference systems (AHRS) provide pitch and roll angles relative to the earth gravity vector, and heading (azimuth) angle relative to north. Such systems require an inertial measurement unit (IMU) capable of measuring angular rate and acceleration in three orthogonal axes. Magnetometer augmentation may be employed to improve long term stability. To date, angular rate measurement is typically realized using mechanical, fiber-optic or ring laser gyroscopes. While all three technologies are capable of providing the performance required for AHRS systems, they all have limitations in realizing low production cost solutions. In contrast Micro-Electro-Mechanical Systems (MEMS), produced using batch processes, have the potential to substantially lower the cost of an AHRS system. For more than a decade MEMS sensors capable of measuring acceleration and angular rate have been very common in many other fields of application such as automotive safety systems and consumer electronics [1]. However, while MEMS accelerometers have been successfully used in AHRS systems [2] this field has to date remained a challenge for MEMS gyroscopes.

To our knowledge no AHRS utilizing MEMS gyros has been qualified according to the Federal Aviation Administration (FAA) Technical Standard Order C5e (TSO-C5e) for the directional gyro (DG) mode of operation. DG mode is required for many applications including large commercial aircraft, flights close to the magnetic north pole and helicopter flights to and from oil rigs or other large metal structures. IMUs used for DG mode operation require that the overall error should not exceed 5 °/h (1 σ). In contrast, typical automotive sensors are specified in degrees per second. AHRS accelerometers require an overall error not exceeding 2.5 mg (1 σ).

The overall bias error of MEMS gyroscopes is composed of errors due to changes of the sensor's environment, i.e. temperature, vibration, and acoustic noise. In typical AHRS environments the levels of vibration and acoustic noise are moderate and the challenge is primarily to obtain sufficiently low temperature errors. For the potential use of the IMU in derivative applications with harsher environmental conditions (e.g. tactical missiles) it becomes essential to design the sensor element for high robustness against vibrational and acoustic disturbance while maintaining low temperature sensitivity.

## II. MEMS Gyroscope

MEMS gyroscopes have been developed and demonstrated for almost two decades [1] and are widely used in automotive and consumer applications. Recently published MEMS gyroscopes [3] have shown significantly improved performance in angular random walk (ARW) and bias instability (i.e. flicker noise, sometimes called bias drift). However, MEMS gyroscopes have had difficulty in combining excellent ARW and bias instability with other requirements, including bandwidth

1-4244-1537-3/08/$25.00 ©2008 IEEE

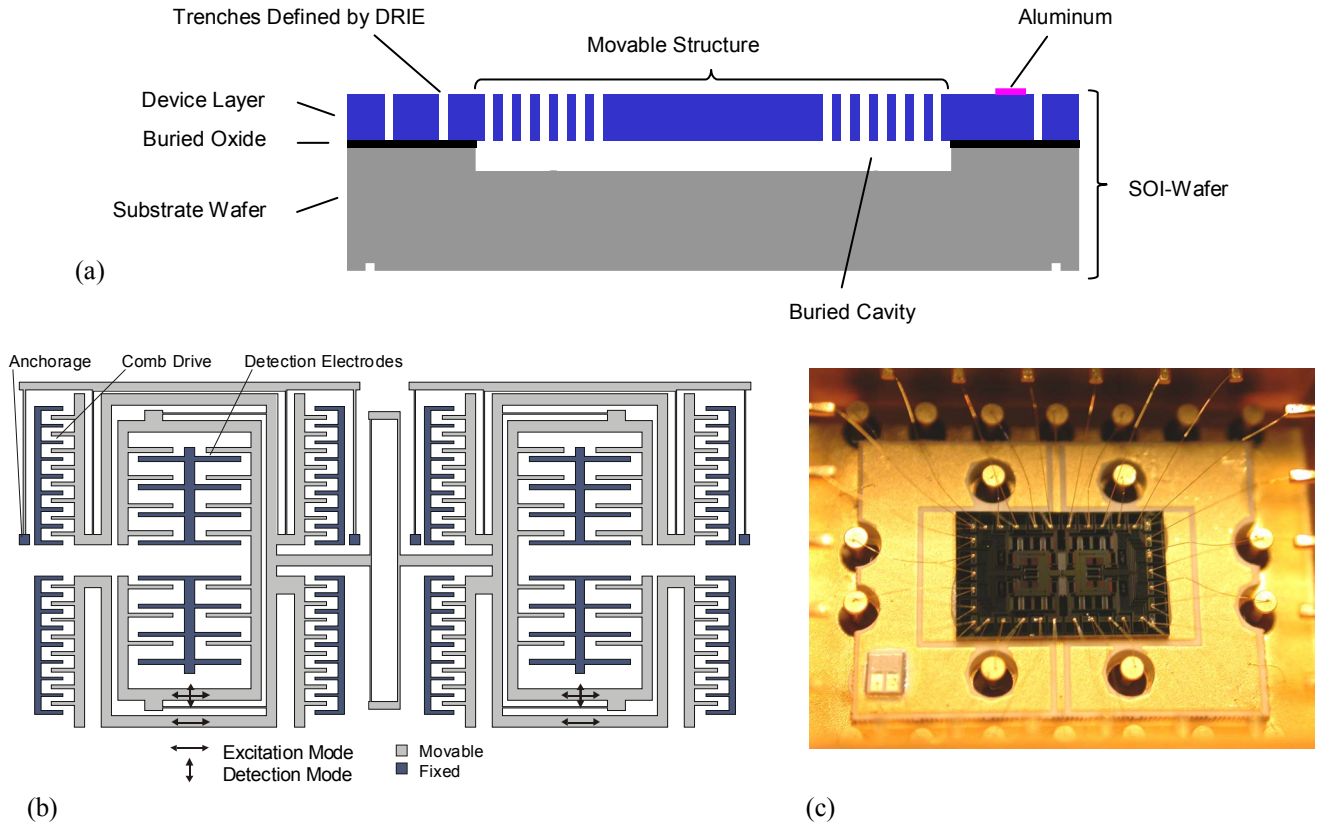


Fig. 1: (a) Schematic cross section of uncapped sensor die. One DRIE step is used to structure movable mass, spring structures, torquer and pick-off electrodes. (b) Schematic top-view of the sensitive element and (c) micrograph of assembled chip without cover wafer.

and temperature stability. The concept below, which was first presented at [4], describes an avionics/tactical grade IMU using closed-loop MEMS gyroscopes.

### *A. Basic Concept*

A schematic cross section of the uncapped sensor gyroscope is shown in Fig. 1 (a) together with a schematic top-view in Fig. 1 (b) and a micrograph of the device in Fig. 1 (c). The operational principle of the MEMS silicon gyroscope is based on a modified tuning-fork configuration with two in-plane oscillation modes. The excitation and the detection mode of the so-called "Dual Linear Configuration" (DLC) are made up of two orthogonal, linear antiphase oscillators. Because of the permanently driven excitation a rotation rate around an axis perpendicular to the plane defined by these two oscillation modes results in Coriolis forces driving the detection oscillation. Various comb structures are used as electrostatic torquer elements and as capacitive pick-offs. This allows the control of the excitation oscillation and the rebalance of the Coriolis force and quadrature.

Recall the objective to achieve the required precision of 5 °/h. This means several key challenges have to be dealt with, which can be illustrated with the following rough estimate. During the drive oscillations the excitation mode is typically exposed to accelerations of approximately 4000 g. Rotating the sensor around its sensitive axis with 5 °/h creates oscillating Coriolis acceleration in the lower µg range. Thus any unwanted time varying coupling effects between the excitation and detection mode have to be smaller than a factor of $10^{-9}$. A detailed analysis of a sensor error model has identified four main requirements for a vibrating MEMS gyroscope capable of 5 °/h [4]:

(i) Closed-loop operation of excitation and detection mode
(ii) Mechanical quality factors Q >> 1000
(iii) Perfect mode matching between excitation and detection modes
(iv) Auxiliary control loops for compensation of fabrication tolerances that create unwanted mode coupling effects

Deep Reactive Ion Etching (DRIE) is used as the key technology for the fabrication of the all silicon gyroscope. Electrode gaps of 2.5 µm and a device layer thickness of 50 µm are realized. Through silicon fusion bonding a pressure smaller than $3 \cdot 10^{-2}$ mbar is encapsulated. In Fig. 2 the measured long term stability of the enclosed pressure is shown. By measuring the Q-factor the enclosed pressure was monitored for three

different samples, which have been bonded in June 2003. Within the measurement accuracy the pressure turned out to be stable for all samples over the test period of 1800 days.

### *B. Signal Processing Concept*

The basic concept of the gyro signal processing realizes the excitation and detection modes of the gyro in a form of closed-loop operation. Fig. 3 depicts the four main control loops associated with the regulation of the mechanical modes. One control loop keeps the excitation mode x1 oscillating with constant amplitude of velocity. The pick-off signal is demodulated with cosine/sine (DEMOD) and lowpass-filtered (LP) to derive phase/frequency information and amplitude information. Regulator outputs drive a variable frequency oscillator (PLL) and modulated torquer signals (MOD) respectively. A similar scheme is applied to the detection mode x2 to rebalance Coriolis forces (I-REGULATOR) and quadrature (Q-REGULATOR).

In order to adjust the resonant frequency of the detection mode to the resonant frequency of the excitation mode an adjustable electrostatic spring is controlled by an auxiliary regulator (FAUX-REGULATOR). Its operation is based on an auxiliary signal (FAUXSIGGEN) injected into the quadrature channel and rotated in phase by 90° through the gyro sensor's transfer function. The response is therefore demodulated (FAUXDEMOD) at the rate channel output

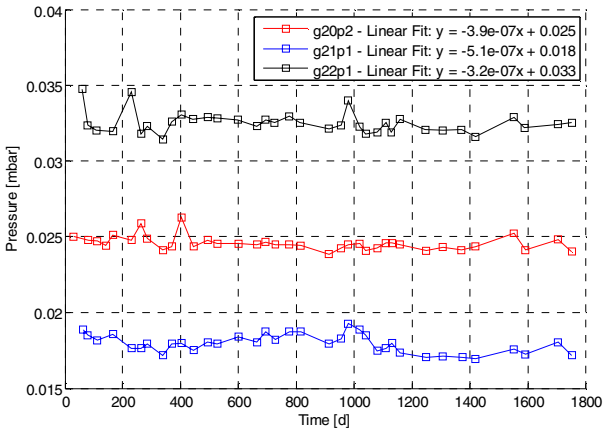


Fig. 2: Measurement of the long term stability of the enclosed pressure for three different gyroscope samples, which have been bonded in June 2003.

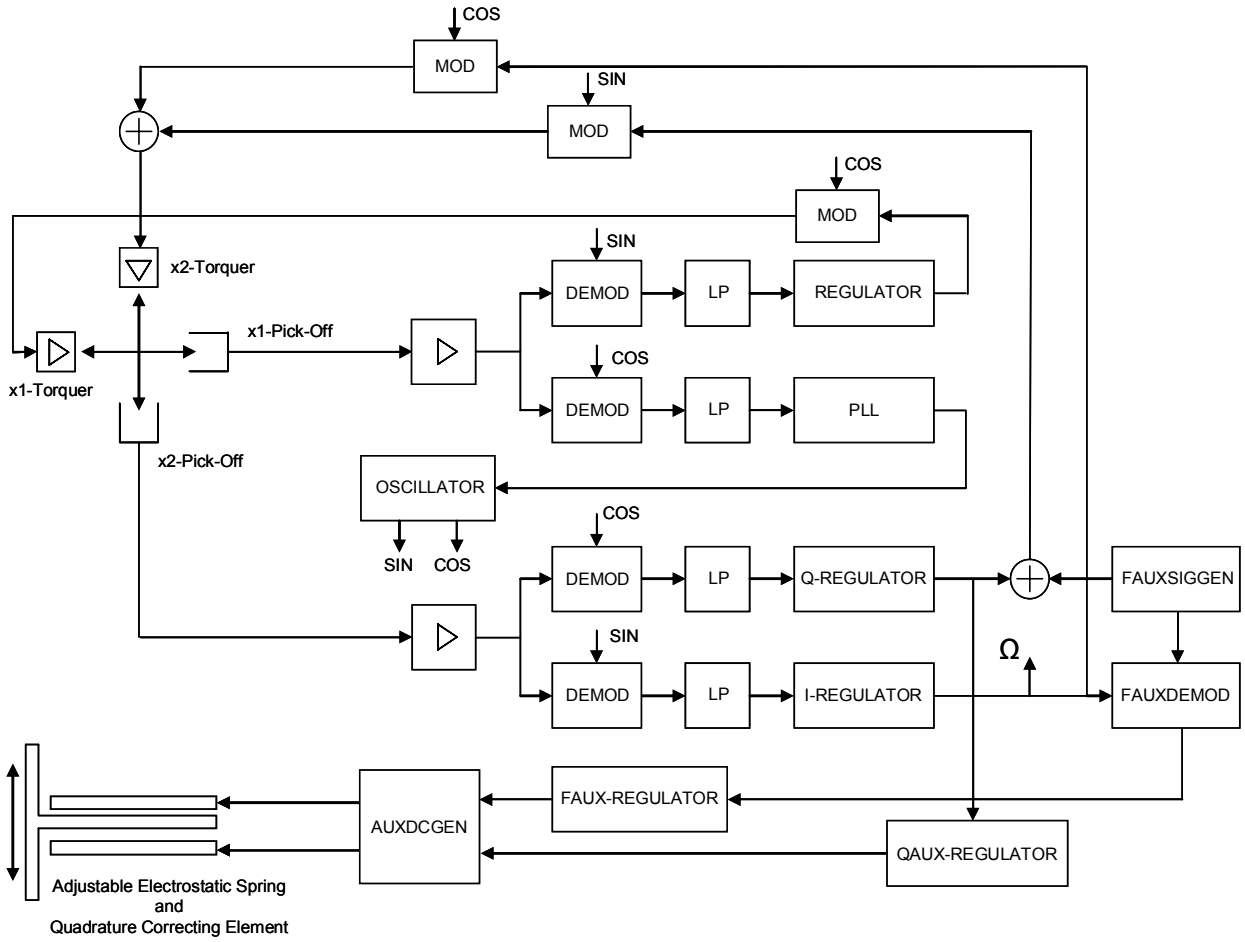


Fig. 3: Block diagram of gyro signal processing and control loops.

(I-REGULATOR). The actuator element AUXDCGEN generates electrostatic DC-forces which are used for two purposes, (i) the adjustable spring and (ii) for quadrature compensation. The latter is based on a second auxiliary control loop with the auxiliary regulator (QAUX-REGULATOR) receiving its input signal from the quadrature regulator's output signal (Q-REGULATOR).

### C. *Gyroscope Performance*

One distinguishing feature of the MEMS gyroscope is its bandwidth of >500 Hz, determined by closed loop transfer function measurements.

Noise analysis was carried out using Allan-Variance as the standard assessment tool. Fig. 4 shows an example Allan plot at room temperature. Up to cluster times $\tau$ greater than 2000 s the slope -1/2 indicates angle random walk of 0.3 °/√h as the predominant noise characteristic. The bias instability can be read off at approximately 20 h as 0.12 °/h (the measurement time was 130 h).

The measurement range of the gyroscopes is adjustable and is set to ±1000 °/s. Typical nonlinearities of the scale factor are below 400 ppm.

The IMU has to be able to operate and maintain the required performance while being subjected to changes in (i) temperature, (ii) vibration and (iii) acoustic noise. The performance of single axis gyroscopes under the influence of varying environmental conditions is shown exemplarily in the following.

At [5] we presented a single axis gyroscope with a 1 σ-error under 5 °/h over the temperature range from -40 °C to +85 °C. This figure has been further reduced by advances in the fabrication process. Fig. 5 shows the filtered (100 s moving average) and temperature compensated (3rd order model) rate output for a gyroscope subjected to twelve temperature cycles

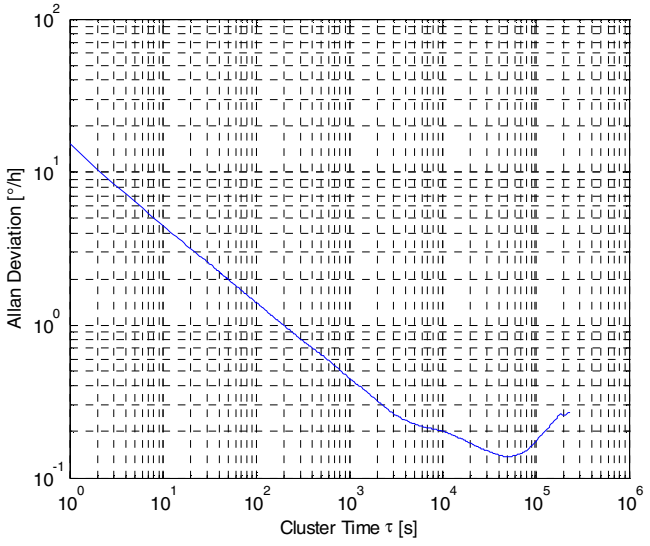


Fig. 4: Allan Standard Deviation of a single axis gyroscope over a period of 130 h with a sample rate of 1 Hz.

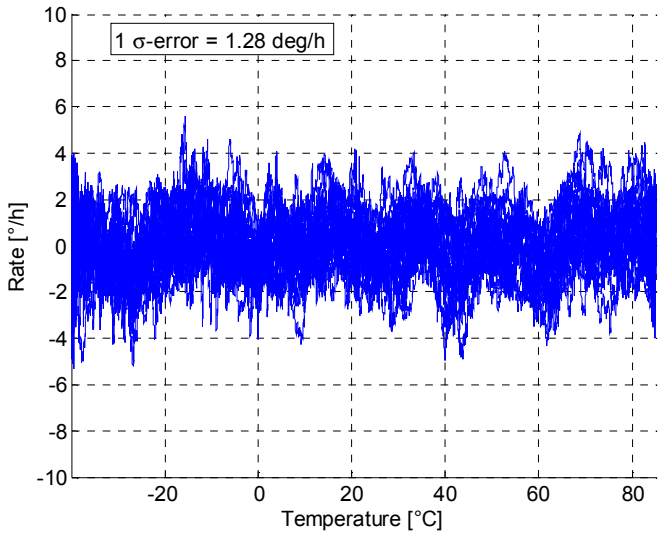


Fig. 5: Single axis gyroscope measured over 62 h with twelve temperature cycles from -40°C to +85°C with temperature slopes varying from 0.5 K/min to 3 K/min. The data are filtered with a 100 s moving average filter and compensated with a 3rd order temperature model with a remaining bias error (1 σ) of 1.28 °/h.

over 62 h. These cycles have varying temperature slew rates from 0.5 K/min to 3 K/min. The remaining 1 σ-error is 1.28 °/h. Furthermore it should be noted that the signal shows no measurable drift within the time period. These sensors are therefore well suited for applications requiring 5 °/h accuracy with sufficient performance margin to accommodate further errors.

Scale factor errors of the single axis gyroscopes over the above given temperature range are measured at discrete temperature levels with stabilized temperature. Typical scale factor errors are in the range of 200 ppm to 1200 ppm.

A critical error source for all mechanical sensors is vibration. At the beginning of our development vibration rectification was a major issue [5]. The following measurement results show that the vibration induced errors could be reduced to values, which result in bias errors <5 °/h at vibration levels of 15 $g_{rms}$.

For AHRS applications typical spectral requirements are defined in DO160-D, section 8, curve B, resulting in an effective vibration acceleration of 1.48 $g_{rms}$. Fig. 6 shows the rate output of a sensor submitted for 10 minutes to 0%, 50%, 100%, and 0% of this spectrum. The measured amplitude of the vibration rectification term, which is dependent upon process tolerances, meets the requirements of an AHRS application.

Design improvements were implemented to meet application requirements with higher levels of vibration. For the corresponding tests a constant vibration spectral power density between 20 Hz to 2 kHz is applied. The vibration levels are increased by 1 $g_{rms}$ between 5 $g_{rms}$ and 15 $g_{rms}$. For high accuracy of the bias measurement, each vibrational amplitude is maintained for 80 min. At the beginning, at the end, and be-

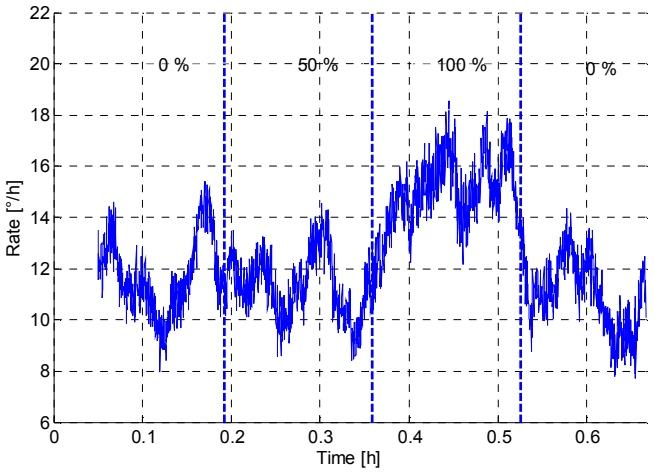


Fig. 6: Rate signal of a single axis gyroscope under vibration according to DO160-D, section 8, spectral shaping curve B applied with 0%, 50 %, 100%, 0% for 10 minutes each.

tween each increase the vibration level is set to 0 $g_{rms}$. The upper graph in Fig. 7 corresponds to rate data accumulated over 1 s, the lower graph shows the data filtered over 100 s (moving average). Within the measurement accuracy neither a bias shift nor a significant change of the output noise under vibration is detectable. The resulting vibration rectification error is smaller than 0.02 °/h/g².

Acoustic noise measurements were performed according to MIL-Standard 810E and DEF-Standard 00-35, Part 3. For engineering tests an acoustic chamber was built, which allows applying sound pressure levels within the relevant frequency

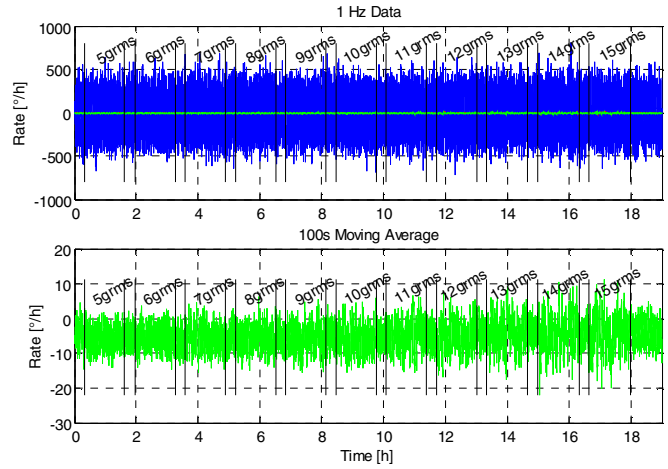


Fig. 7: Rate signal of single axis gyroscope under vibration with constant vibration spectral power density between 20 Hz to 2 kHz. The vibration levels are increased by 1 $g_{rms}$ between 5 $g_{rms}$ and 15 $g_{rms}$. At the beginning, at the end, and between each increase the vibration level is set to 0 $g_{rms}$. The upper graph corresponds to data accumulated over 1 s, the lower graph to data filtered over 100 s (moving average).

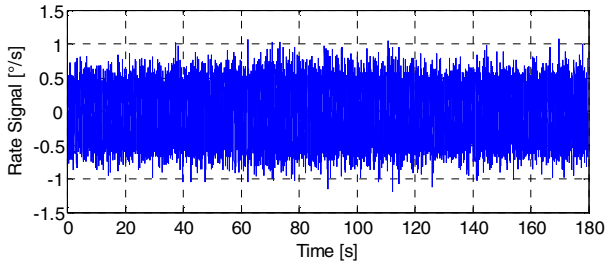


Fig. 8: Rate signal of a single axis gyroscope under acoustic noise corresponding to an overall sound pressure level of 140 dB ( 0%, 100 %, 0% for 60 s each; data rate of 666 Hz).

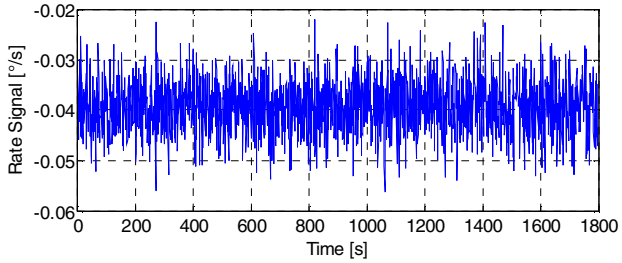


Fig. 9: Rate signal of a single axis gyroscope under acoustic noise corresponding to an overall sound pressure level of 140 dB ( 0%, 100 %, 0% for 600 s each; data accumulated over 1 s).

bands corresponding to overall sound pressure levels above 140 dB (referred to 20 µPa). The critical frequency bands are determined by frequency sweeps. Fig. 8 shows the rate signal under acoustic noise, at the beginning and at the end at a level of 0 dB for 60 s in each case, and in the middle for 60 s at a level corresponding to a broadband overall sound pressure level of 140 dB. The data rate was 666 Hz. This measurement demonstrates that the sensor noise is not affected by the acoustic noise. The impact on the bias is shown in Fig. 9. For sufficient accuracy the measurement was performed over a period of 30 min (10 min 0 dB, 10 min corresponding to 140 dB, and 10 min 0 dB) and the data were accumulated over 1 s. The resulting bias error is smaller than 1 °/h.

## III. MEMS Accelerometer

LITEF started fabricating MEMS based accelerometers for commercial aviation applications in the early 1990s [2]. These capacitive, pendulum type sensors were fabricated using silicon wafers in combination with an anisotropic wet etching process. Operated in closed-loop mode, the accelerometers have achieved the performance required for AHRS systems and are currently used in a wide range of our products. While retaining the same control concept developed for these wet etched sensors, the MEMS accelerometer chip used in this IMU is based on the DRIE all silicon technology of the MEMS gyroscope. This approach promises the reduction of production costs and size of the sensor while being capable of achieving the accuracy required for AHRS applications. For first measurements the measurement range was set to ±15 g,

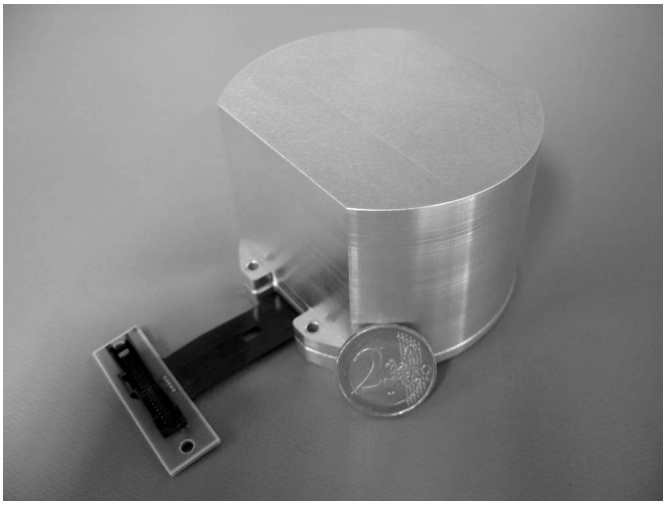

Fig. 10: Photograph of the MEMS IMU.

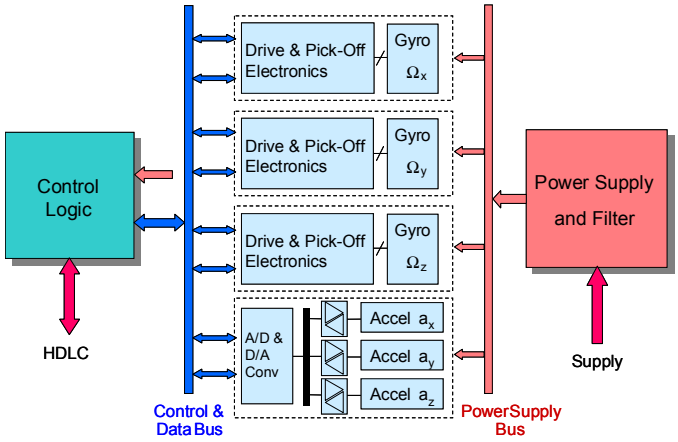


Fig. 11: Block Diagram of the MEMS IMU.

whereas stable operation up to ±55 g was demonstrated. By closed loop transfer function measurements a sensor bandwidth >800 Hz is obtained. Further results are shown in paragraph IV.C.

## IV. General Concept of the MEMS IMU

The MEMS IMU comprises three MEMS accelerometers and three MEMS gyroscopes, which together with the required supporting analog electronics and digital control logic are packaged with appropriate measures for thermal, acoustic and vibration management within an outline of 85 mm in outer diameter and 60 mm in total height. The photograph of a prototype IMU depicted in Fig. 10 shows a single piece cover screwed together with a base plate, and a flex with test connector. The final version of the IMU will feature the same outline, but will be hermetically sealed to ensure long term stability and will have a connector panel directly on top of the cover.

### *A. Challenges*

Integrating MEMS accelerometers and MEMS gyros into a multi-sensor IMU presents several challenges. For example, as a result of parameter variations during the production process, mechanical frequencies of the sensors differ. As a consequence intermodulation interferences in mechanical and/or electrical domains are an issue that has to be dealt with. Furthermore, packing the six sensors and the surrounding electronics in a small volume generally increases power dissipation per unit of volume, thus increased sensor and electronics self-heating have to be considered.

Concepts for mechanical decoupling to mitigate vibration and acoustic sensitivity tend to interfere with concepts for thermal management or electrical conductivity and shielding. Therefore mechanical and electrical connectors need to be carefully selected with respect to material properties and size.

Having characterized the sensors in single axis systems, it is possible to benchmark the IMU performance and compare with the previously achieved single axis results. This enables the differentiation between various sources of error.

### *B. MEMS IMU Architecture*

A block diagram of the MEMS IMU architecture is depicted in Fig. 11. Gyro and accelerometer sensors are controlled by digital logic including digital signal processing and interfaces that share common digital buses. Analog sensing electronics are positioned next to the MEMS sensor chips. Measures to decouple supply voltages and minimize sensor interference are implemented in the design.

The interface to the host system is based on an asynchronous HDLC protocol. Frame rates of 1024 Hz can be achieved to fully exploit the high sensor bandwidths. A single power supply voltage is sufficient to power all components of the IMU.

### *C. First IMU Results*

This paragraph gives some examples of the first results obtained with the MEMS-IMU at measurements over the temperature range from -10°C to +50°C. For most measurements the residual 1 σ-error after compensation with a 3rd order temperature model is given. Differing analysis or temperature range will be noted.

Due to appropriate mechanical design the maximum uncompensated misalignment error over temperature of the three gyroscopes and three accelerometers is well below 0.1 mrad.

Scale factor errors of the gyroscopes and the accelerometers are in the same range as obtained with single axis sensors. For the measurements belonging to Fig. 12 the residual errors are smaller than 450 ppm for all three gyroscopes. The results of the accelerometers are depicted in Fig. 13. All three axes have errors below 700 ppm.

The residual errors over the temperature range of -40°C to +85°C for the three acceleration sensors of the MEMS IMU are shown in Fig. 14. The 1 σ-error is smaller than 1 mg and therefore well within the 2.5 mg design goal.

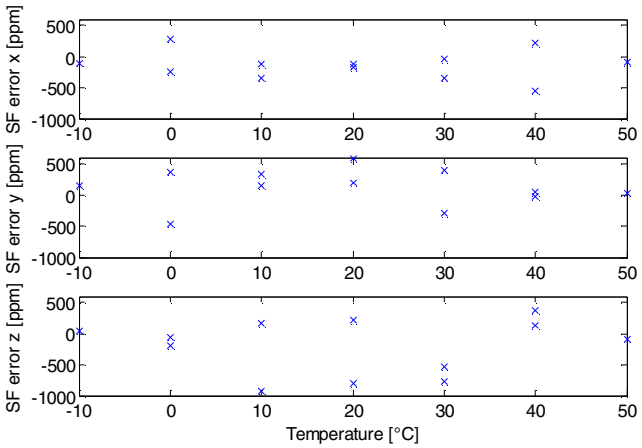


Fig. 12: IMU gyroscope scale factor error vs. temperature. The 1 σ-error with a 3rd order temperature model is smaller than 450 ppm for all three axes.

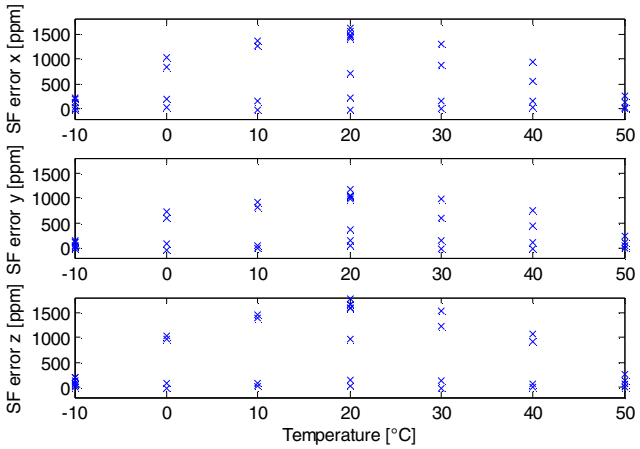


Fig. 13: IMU accelerometer scale factor error vs. temperature. The 1 σ-error with a 3rd order temperature model is smaller than 700 ppm for all three axes.

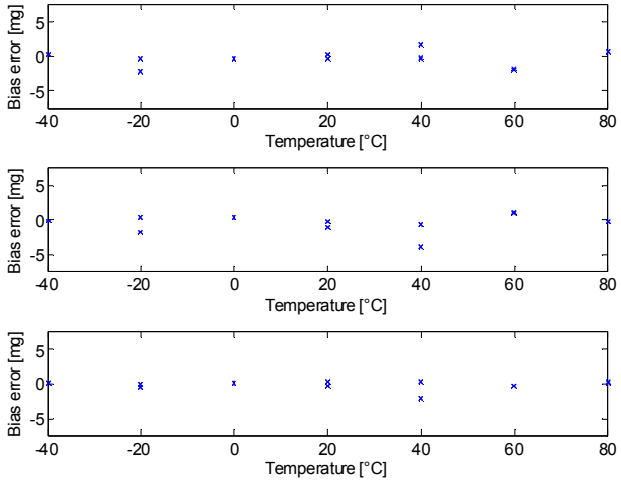


Fig. 14: IMU accelerometer bias vs. temperature. The 1 σ-error with a 3rd order temperature model is smaller than 1.0 mg for all three axes.

## V. Conclusion

The comparison of measurement results with design goals in Table I shows that we have successfully designed and implemented the concept and technology of a MEMS IMU based on silicon DRIE etched gyroscopes and accelerometers. Due to the use of closed-loop control systems and the minimization of sensitivity to changes of temperature, vibration and acoustic noise, the IMU is capable of meeting the requirements of an AHRS system operating in DG mode as well as the requirements of applications with higher levels of vibration and acoustic noise (e.g. tactical missiles).

## References

[1] N. Yazdi, F. Ayazi, and K. Najafi, *Micromachined Inertial Sensors*, Proc. IEEE, vol. 86, no. 8, pp. 1640-1659, Aug. 1998.

[2] M. Hafen, E. Handrich, W. Gutmann, B. Ryrko, G. Spahlinger, E. Vetter, *Hochgenauer Beschleunigungsmesser B-290 in Mikrotechnologie*, Kongress Sensor 93, Nürnberg, 11.-14.10.1993

[3] A. Sharma, M.F. Zaman, M. Zucher, and F. Ayazi, *A 0.1°/hr Bias Drift Electronically Matched Tuning Fork Microgyroscope*, Tech. Dig., IEEE MEMS '08, Tucson, AZ, USA, 2008, pp. 6-9.

[4] W. Geiger, et al., *The Micromechanical Coriolis Rate Sensor µCORS II*, Symposium Gyro Technology 2003, Sep. 2003, Stuttgart, Germany, pp. 5.0-5.9.

[5] S. Zimmermann, et al., *Single Axis Gyroscope Prototype based on a Micromechanical Coriolis Rate Sensor*, Symposium Gyro Technology 2006, Sep. 2006, Stuttgart, Germany, pp. 9.0-9.9.

TABLE I
PERFORMANCE PARAMETERS

| Parameter | Measurements (Typical Values) | Goals |
|---|---|---|
| **Gyroscopes** | | |
| Measurement Range [°/s] | ±1000 | ±1000 (±3000) [b] |
| Bias Error over Temperature (1 σ) [°/h] | 1.0 … 5.0 [a] | <5 |
| Scale Factor Error over Temperature (1 σ) [ppm] | 200 … 1200 | <1000 |
| Misalignment Error over Temperature (max.)[mrad] | <0.1 | <0.5 |
| Angular Random Walk [°/√h] | 0.2 … 0.4 [a] | <0.3 |
| Vibration Rectification Error (1 σ) [°/h/g²] | <0.02 [a] | <0.3 |
| Acoustic Rectification Error at 140 dB [°/h] | <1.0 [a] | <5 |
| Bandwidth [Hz] | 500 | >250 |
| **Accelerometers** | | |
| Measurement Range [g] | ±15 (±55) [b] | ±30 (±70) [b] |
| Bias Error over Temperature (1 σ) [mg] | 0.50 … 2.0 | <2.5 |
| Scale Factor Error over Temperature (1 σ) [ppm] | 400 … 1400 | <1500 |
| Misalignment Error over Temperature (max.) [mrad] | <0.1 | <0.5 |
| Bandwidth [Hz] | 800 | >500 |

[a] Single axis measurements, IMU measurements ongoing.
[b] Other performance parameters may vary with increased range.